ROYAL SOCIETY OF CHEMISTRY

Journal of
Materials Chemistry A

Tetrazole substituted polymers for High Temperature Polymer Electrolyte Fuel Cells

Journal:	*Journal of Materials Chemistry A*
Manuscript ID:	TA-ART-03-2015-001936.R3
Article Type:	Paper
Date Submitted by the Author:	01-Jun-2015
Complete List of Authors:	Henkensmeier, Dirk; Korea Institute of Science and Technology, Fuel Cell Research Center Duong, Ngoc My Hanh; KIST, Brela, Mateusz; Jagiellonian University, Theoretical Chemistry Dyduch, Karol; Jagiellonian University, Theoretical Chemistry Michalak, Artur; Jagiellonian University, Theoretical Chemistry Jankova, Katja; DTU, Energy Cho, Hyeongrae; KIST, Jang, Jong Hyun; Korea Institute of Science and Technology, Fuel Cell Research Center Kim, Hyoung-Juhn; Korea Inst Sci & Technol , Fuel Cell Research Center Cleemann, Lars; Technical University of Denmark, Li, Qingfeng; Technical University of Denmark, Department of Energy Conversion and Storage Jensen, Jens Oluf; Technical University of Denmark,

SCHOLARONE™
Manuscripts

Tetrazole substituted polymers for High Temperature Polymer Electrolyte Fuel Cells

Dirk Henkensmeier,[a,b]* Ngoc My Hanh Duong,[a,b] Mateusz Brela,[c] Karol Dyduch,[c] Artur Michalak,[c*] Katja Jankova,[d] Hyeongrae Cho,[a] Jong Hyun Jang,[a,e] Hyoung-Juhn Kim,[a] Lars N. Cleemann,[d] Qingfeng Li,[d] Jens Oluf Jensen[d]

a) Korea Institute of Science and Technology, Fuel Cell Research Center, Hwarangno 14-gil 5, 136-791 Seoul, Republic of Korea
b) University of Science and Technology, 217 Gajungro, Yuseonggu, Daejeon, Republic of Korea
c) Jagiellonian University, Faculty of Chemistry, Ingardena 3, 30-060 Krakow, Poland
d) Proton Conductors, DTU Energy, Technical University of Denmark, Kemitorvet 207, DK-2800 Kgs. Lyngby, Denmark
e) Green School, Korea University, Seoul 136-713, Republic of Korea
* corresponding authors; email: henkensmeier@kist.re.kr; Tel. +82-2-958-5298.
michalak@chemia.uj.edu.pl; Tel. +48-12-6632217.

Abstract

While tetrazole (TZ) has much lower basicity than imidazole and may not be fully protonated in the presence of phosphoric acid (PA), DFT calculations suggest that the basicity of TZ groups can be increased by introduction of a 2,6-dioxy-phenyl-group in position 5 of TZ. This structure allows hydrogen bonds between TZ protons and ether oxygen atoms, and thereby establishes a resonance stabilised, co-planar structure for tetrazolium ions. Molecular electrostatic potential (MEP) calculations also indicate that tetrazolium ions possess two sites for proton hopping. This makes such materials interesting for use in a high temperature fuel cell (HT PEMFC). Based on these findings, two polymers incorporating the proposed TZ groups were synthesised, formed into membranes, doped with PA and tested for the fuel cell relevant properties. At room temperature, TZ-PEEN and commercial *meta*-PBI showed an equilibrium uptake of 0.5 and 4.7 mol PA/mol heterocycle, indicating that PBI has higher affinity to PA then TZ-PEEN. The

highest achieved PA uptake was ca. 110 wt%, resulting in a proton conductivity of 25 mS/cm at 160 °C with a low activation energy of about 35 kJ/mol. In a first HT PEMFC test at 160 °C, a peak power density of 287 mW/cm^2 was achieved.

Keywords: HT PEMFC, tetrazole, polyether, membranes, phosphoric acid doping

1. Introduction

High temperature polymer electrolyte membrane fuel cells (HT PEMFCs) are operating in the temperature range of 120-200 °C. The gas streams are usually unhumidified, but can also contain water if the cell is connected to a reformer.[1] Since no liquid water exists under these conditions (unless a very high pressure is applied), the electrolyte is usually based on phosphoric acid (PA). In contrast to phosphoric acid fuel cells (PAFCs) where an inorganic e.g. SiC matrix is used to immobilize liquid PA, HT PEMFCs employ PA absorbed in a dense polymeric membrane. The most common membrane type is PA doped polybenzimidazole (PBI), in which PA interacts with the basic nitrogen atoms of the imidazole rings.[2] While only one PA molecule interacts strongly with an imidazole ring, several more PA molecules can be absorbed by hydrogen bonding. Up to 5- 6 PA molecules per imidazole can be doped when *meta*-PBI is immersed in 85 wt% PA solution at room temperature.[3] Membranes prepared by a sol-gel process, in which PBI precipitates out of a polyphosphoric acid (PPA) solution as the temperature is decreasing and PPA is hydrolysed by ambient humidity to PA, can even keep up to about 20 molecules PA per imidazole.[4]

So far, most published work has been dedicated to PBI based systems,[5] and there is only limited work on alternative polymers. The most advanced alternatives probably are aromatic poly(ethers) incorporating pyridine moieties in the backbone.[6-8] Some researchers also reported the use of imidazole moieties as a side group in aromatic polymers,[9] or as part of radiation grafted polymers[10]. Considering the large variety of nitrogen containing heterocycles which could be attached to polymers, it is surprising that literature is rather scarce on other heterocycles than imidazole or pyridine. However, there is a small body of literature on tetrazole containing polymers, which were doped with PA and characterised for their fuel cell relevant ex-situ properties.[11, 12] Very recently, Song et al. showed the fuel cell performance of PA doped tetrazole containing polymers.[13] Inspired by this work, we now present the preparation and

properties of poly(arylene ethers) with tetrazole moieties attached to the backbone. Theoretical modeling has been recently successfully applied in studies focused on proton exchange membranes. [14-16]. In this work Density Functional Theory (DFT) calculations are applied to describe geometry and the electronic structure of tetrazole based polymer models, compared with the corresponding PBI models. In particular we discuss the charge distribution and its implications for possible protonation sites and the protonation energies. The calculations suggest that 5-(2,6-oxy-phenyl)-based tetrazoles have especially attractive properties. Finally, we also tested the new materials in the fuel cell, and while Song et al. operated their cells only up to 120 °C,[13] we show that tetrazole based fuel cell membranes can be operated also at 160 °C.

2. Experimental section

2.1 Polymer synthesis

2.1.1 Materials

Dimethyl sulfoxide (DMSO) was obtained from Daejung, dimethyl sulfoxide-d_6 (DMSO-d_6, 99.9% D) was obtained from Cambridge Isotope Laboratories, 2,6-difluorobenzonitrile from Oakwood products. 2-methylhydroquinone, bisphenol A, hydroquinone sulfonic acid potassium salt, sodium azide (NaN$_3$), zinc cloride (ZnCl$_2$), dimethylacetamide (DMAc), N-Methyl-2-pyrrolidone (NMP), toluene, potassium carbonate (K$_2$CO$_3$) were obtained from Sigma. All chemicals were used without further purification.

2.1.2 Synthesis of PEEN (Poly (ether ether nitrile))

In a three-necked round-bottom flask, fitted with stirrer and a Dean-Stark Trap, 2.78 g (20 mmol) 2,6-difluorobenzonitrile, 2.48 g (20 mmol) 2-methylhydroquinone and 5.52 g potassium carbonate (K$_2$CO$_3$) were dissolved in a mixture of 35 ml anhydrous dimethylacetamide (DMAc) and 31 ml anhydrous toluene. After thorough flushing with nitrogen, the mixture was then heated under stirring at 150 °C for 4 hours, in order to remove the water by azeotropic distillation with toluene. When toluene was completely removed, the suspension was heated at 180 °C until the viscosity visibly increased. The reaction mixture was cooled down, the polymer precipitated in DI water, washed for 24 hours and dried in vacuum at 60 °C for 48 hours. PEEN is soluble in hot NMP, but not well soluble in chloroform, DMSO, DMSO/chloroform, DMSO/0.5wt% LiCl and tetrahydrofurane.

2.1.3 Synthesis of SPEEN (sulfonated Poly-(ether ether nitrile sulfone))

2.78 g (20 mmol) 2,6-difluorobenzonitrile, 2.74 g (12 mmol) bisphenol A, 1.83 g (8 mmol) hydroquinone sulfonic acid potassium salt 5.52 g, potassium carbonate (K_2CO_3) were dissolved in a mixture of 25 ml anhydrous dimethylacetamide (DMAc) and 31 ml anhydrous toluene. After thorough flushing with nitrogen, the mixture was heated under stirring at 150 $^{\circ}$C for 4 hours, in order to remove the water by azeotropic distillation with toluene. When toluene was completely removed, the suspension was heated at 170 $^{\circ}$C until the viscosity visibly increased. The reaction mixture was cooled down, the polymer precipitated in DI water, washed for 24 hours and dried under reduced pressure at 60 $^{\circ}$C for 24 hours. ^{1}H NMR (300 MHz, DMSO-d_6, ppm): 7.19-7.62 (m, ca. 70H, aromatic protons of BPA (7.38 and 7.19 ppm), the hydroquinone sulfonic acid moiety, and the proton in *para*-position to nitrile), 6.43-6.77 (m, ca. 20H, aromatic protons in *meta*-position to nitrile), 1.73 (s, 36H, BPA -CH_3).

2.1.4 Preparation of tetrazole-containing PEEN, SPEEN (TZ-PEEN, TZ-SPEEN)

TZ-PEEN, TZ-SPEEN were prepared and optimized by [2+3] addition reaction.[17] First, 1 g PEEN or SPEEN was dissolved in 24 ml NMP at 140 $^{\circ}$C. NaN$_3$ and anhydrous ZnCl$_2$ with the molar ratio of –CN/ZnCl$_2$/NaN$_3$ 1:4:4 were introduced later into the flasks. The reaction mixtures were stirred at 140 $^{\circ}$C for a total of 6 days. The withdrawn samples were heated at 60 $^{\circ}$C for 1 hour in dil. HCl, filtered, washed on the filter with the dil. HCl followed by water, and then dried under reduced pressure at 60 $^{\circ}$C for 24 hours.

2.2 Polymer Characterization

Chemical structures were characterized using a Bruker 300 MHz nuclear magnetic resonance (NMR) spectrometer.

FT-IR spectra were recorded on a Lambda Scientific FTIR 7600 spectrometer with a single bounce diamond ATR accessory with film samples at 4 cm^{-1} resolution, 16 scans, over the 400-4000 cm^{-1} range.

2.3 Membrane fabrication and acid doping

TZ-PEEN and TZ-SPEEN were dissolved in NMP to obtain 5% wt. solutions at room temperature. The solutions were then filtrated through polypropylene filters (pore size 0.45 μm) into petri dishes and dried at 60 °C, first under ambient pressure for 1 hour, later under vacuum for 24 hours.

The acid doping of the membranes was performed by immersing the membranes in an 85 wt % PA solution at 30 °C, 80 °C or 120 °C. The PA content was measured based on the weight change of the membrane before and after doping. The PA content (wt%) was calculated according to **Equation 1**, where Wt and Wo are the weights of the membrane after doping and before doping, respectively.

$$\%PA_{uptake} = \frac{W_t - W_0}{W_0} \times 100$$ (**Equation 1**)

2.4 Mechanical testing

Tensile tests were performed on a Cometech QC-508E universal testing machine. The samples were cut from 1 membrane with the sample size of 1 cm x 4 cm, 4 samples were prepared for each kind of membrane. The samples were stretched at the elongation speed of 10 mm/min. For each measurement, humidity and temperature were recorded as the mechanical properties greatly depend on environmental conditions. The maximum stress was taken as the tensile strength.

2.5 Size Exclusion Chromatography

SEC was performed on a Shimadzu HPLC Instrument, equipped with 2 PolarSil columns (100 and 300 Å) from Polymer Standards Service (PSS) and a Shimadzu refractive index detector. The samples were run in DMAC containing 0.5 wt% LiCl at 60 °C at a flow rate of 1 ml/min. Calibration was made with 17 narrow molecular weight PMMA standards from PSS in the molecular weight range of 800 to 1600000 g/mol and the LabSolutions GPC Software.

2.6 Thermogravimetric analysis

Thermal stability of membranes was measured with TA instruments TGA Q50. Sample weights were around 10 mg, and the temperature was increased 10 °C/min from room temperature to 100

°C, kept for 30 minutes, and then again increased at the same heat rate to 900 °C in a nitrogen stream.

2.7 Proton conductivity

A Zahner IM6 impedance analyser (ZAHNER-elektrik GmbH & Co. KG, Kronach, Germany) was used to measure electrochemical impedance spectra of membranes. Membrane samples (4 cm x 1 cm) were doped with phosphoric acid and dried at 110 °C for 5 hours to evaporate water. After that, the membrane was measured in the frequency range of 0.1 Hz to 100 kHz by a 4-probe method. The conductivity σ was calculated according to **Equation 2**.

$$\sigma[mS/cm] = \frac{1000d}{twR}$$ (**Equation 2**)

Here d is the distance between the inner electrodes (1 cm), t and w are the thickness and width (1 cm) of the membrane strip, and R is the resistance [ohm], as obtained from the x-axis intercept of the curve in the Nyquist plot.

2.8 MEA fabrication and fuel cell testing

Catalyst powder (46.3% Pt/C from TKK, Japan) and PTFE dispersion (60 wt% in water from Sigma, Korea) were dispersed in isopropyl alcohol and distilled water (IPA : water = 4:1 wt/wt) with a solid PTFE to Pt/C ratio of 1:4. The catalyst ink was sprayed uniformly onto a gas diffusion layer (SGL GDL 10 BC) to prepare gas diffusion electrodes (GDE) by an automatic spraying machine. The GDEs were then heat treated for 5 minutes at 350 °C under nitrogen atmosphere. The Pt loading on each electrode was 1.03 mg cm^{-2}. The MEAs, with an active electrode area of 7.84 cm^2, were assembled into a single cell without hot pressing, and the screws were fastened with a torque of 80 pound inch (9.04 Nm). The single cells were operated at 160 °C and ambient pressure with non-humidified H$_2$ and air. The gas flow rates were 100 sccm and 300 sccm, respectively. Fuel cell performance was characterized by continuously measuring the potential at constant current (200 mA·cm^{-2}) at 160 °C, and i-V curves.

2.9 Computational details

Theoretical calculations with Density Functional Theory (DFT) methodology using the Becke88 exchange [18] and Perdew86 correlation [19, 20] functional (BP86) were performed using the

Amsterdam Density Functional (ADF) program, version 2013.01[21-25]. A standard triple-ζ STO basis included in the ADF package with one set of polarization functions was applied for all atoms. Scalar relativistic effects were included by employing the Zero Order Regular Approximation (ZORA). [26, 27] Charge distribution was analyzed with the Hirshfeld atomic charges [28] and Molecular Electrostatic Potential [29, 30].

3. Results and Discussion

3.1 Synthesis of tetrazole-modified poly(arylene ether)s

Tetrazoles can be synthesised in a [2+3] cycloaddition of nitrile groups with sodium azide. To enhance the reaction kinetics, usually acidic catalysts are added.[31] While this reaction can be handled well on small scale (e.g. large head space in which hydrazoic acid remains under the detonation threshold of 15,000 ppm), the potential evolution of HN_3 may rise safety issues especially for larger batches.[32] An apparently safe procedure for the kilogram scale was reported by Giradin et al.[33] As shown by Du et al., also aromatic nitrile group containing polymers can react with sodium azide in a polymer analogous reaction.[17] Based on that work, two nitrile containing poly(arylene ethers) were synthesised, hereafter referred to as PEEN and SPEEN (Scheme 1). When fully substituted, PEEN would show a very high density of functional groups, while SPEEN has a slightly lower tetrazole density and an additional sulfonic acid group. The acid group was proposed to improve the conductivity of membranes with a low PA doping level.[34] Characterisation of PEEN and SPEEN was done by NMR spectroscopy. In order to assign the peaks of SPEEN, also a polymer without the hydroquinone sulfonic acid monomer (**P1**) and another polymer without bisphenol A (**P2**) were synthesised and characterised (supporting information). It was found that the protons in *meta*-position to the nitrile group appear at 6.59/6.61 ppm in **P1**, and are split up into signals at 6.91/6.93, 6.77/6.79, 6.63/6.65, 6.48/6.51 and 6.39/6.41 in **P2**, reflecting the 3 possible triades (SO_3H can be *ortho* or *meta* to benzonitrile) and the spatial orientation of the sulfonic acid groups (supporting information).

While the polymerisation reactions easily led to membrane forming polymers, the cycloaddition with azide was very sluggish and reactions needed to be run for several days, as also reported by Du et al.[17] Among the tested conditions (**Table 1**), the highest conversion of the nitrile groups could be achieved when the reactions were run at 140 °C for 6 days in normal (not anhydrous) NMP with zinc chloride as catalyst, in a reagent ratio ($-CN:ZnCl_2:NaN_3$) of 1:4:4. The same

7

reaction conditions were also applied to SPEEN without further optimisation, reaching a nitrile group conversion of about 80% for TZ-SPEEN.
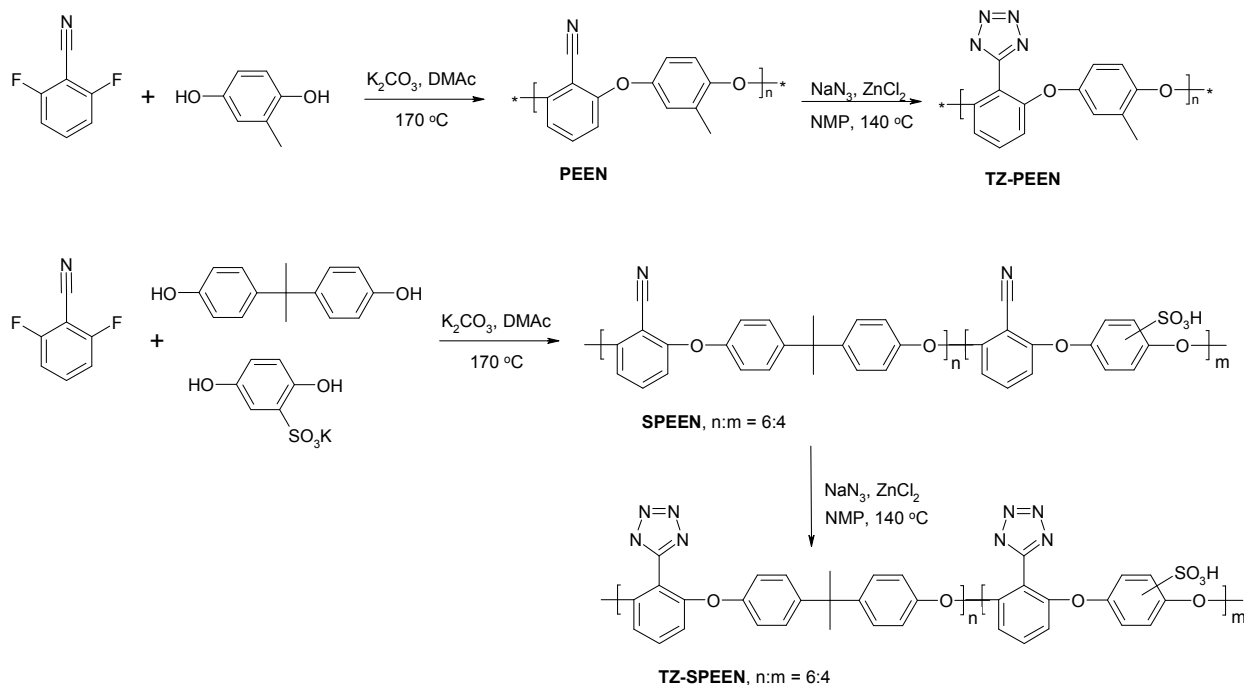
Scheme 1: Synthesis route for polymerisation of PEEN and SPEEN and for post-polymerization modification via [2+3] cycloaddition reaction to introduce tetrazole rings into aromatic polymer backbone (TZ-PEEN and TZ-SPEEN).

Table 1: Reaction conditions tested for PEEN; reaction time 6 days.

Exp. number	Temperature °C	Solvent	Catalyst	Conversion, of nitrile group	Membrane property
1	120	Anhy.NMP	ZnCl$_2$	25%	not casted
2	140	Anhy.NMP	ZnCl$_2$	50%	flexible
3	160	Anhy.NMP	ZnCl$_2$	60%	brittle
4	140	NMP	ZnCl$_2$	70%	flexible

5	140	NMP	AlCl$_3$	30%	not casted

Because the highest turnover reached only around 70 % (TZ-PEEN) and 80% (TZ-SPEEN), the NMR spectra of the tetrazolated polymers were complex and did not allow a detailed characterisation. Nevertheless, a new multiplet appearing at 6.96/6.98 ppm probably stems from the protons in *meta*-position to the tetrazole. ATR FT-IR spectroscopy gave more information. The intensity of the nitrile peaks at 2233 cm^{-1} (PEEN) and 2235 cm^{-1} (SPEEN) decreased with proceeding tetrazolisation. In addition, the bands around 1600 cm^{-1} are slightly broadened and shifted to higher wave numbers. This could indicate the appearance of a new band in this region, since N=N bonds of tetrazoles were reported to give signals around 1600 cm^{-1}.[35] Comparison of the integral areas of the nitrile bands (A$_{CN}$) and the bands around 1030 cm^{-1} as internal standard (A$_{standard}$) allowed calculation of the degree of nitrile conversion, according to **Equation 3**.

$$\text{conversion [\%]} = 100 \cdot (1 - (A_{CN'}/A_{standard'})/(A_{CN}/A_{standard})) \qquad \textbf{(Equation 3)}$$

3.2 Density Functional Theory calculations

The model systems considered in theoretical DFT calculations are shown in **Figure 1**. Starting from the tetrazole structure (**1a),** we further consider a model based on the single repeating unit motif of TZ-PEEN ('monomer' **1b**), saturated by a hydrogen atom (added on phenyl) and a methyl group (linked to the ether oxygen atom**).** Finally, the largest TZ-PEEN model contains three repeating units ('trimer'**1c**, saturated as in the case of 'monomer'). In such a 'trimeric' model as **1c,** the interactions of the central repeating unit with the neighbors are taken into account. A comparison of the results obtained for models **1a**, **1b**, and **1c** allows for discussion of the influence of the ether groups on the properties of the tetrazole fragment, as well as the influence of the neighboring repeating units.
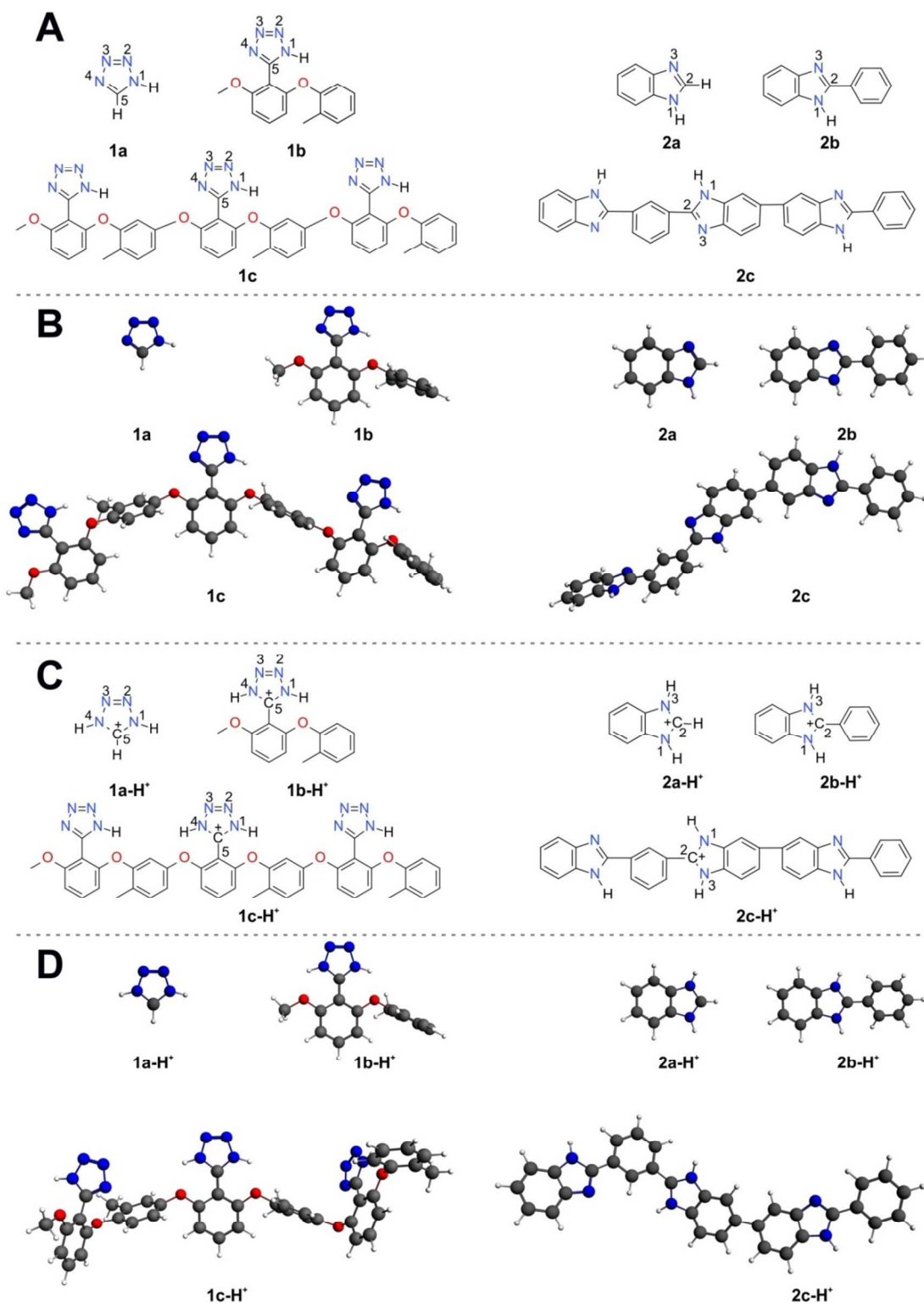
Figure 1: Structures and optimized geometries of studied systems.

The PBI models, used for comparison, were constructed accordingly. We consider benzimidazole (**2a**), 2-phenyl benzimidazole **2b** as 'monomer', and structure **2c** as the 'trimeric' model. It should be noted, however, that the structure **2b** does not directly correspond to the PBI repeating unit, that contains two benzimidazoles linked by the phenyl fragment. The tetrazole-based models **1b** and **1c** include one and three tetrazole fragments, and hence, one and three possible protonation sites, respectively. The main goal of the present analysis was to compare the electronic structure and protonation energies of the tetrazole and PBI polymers, based on comparable models for both systems. Thus, the PBI-models **2b** and **2c** were constructed in such a way that they comprise correspondingly one and three protonation sites, as in **1b** and **1c**. It should be emphasized that in the models based on the 'real' dimer and trimer PBI, the number of the benzimidazole fragments would be 4 and 6, i.e. the number of the protonation sites would be doubled compared to **1b**, and **1c**.

The protonated systems derived from the neutral models are shown in the bottom part of **Figure 1** (part C and D). In all the cases we have considered single protonation; in the case of 'trimeric' models the protonation of the central unit was considered only. Since the electrostatic potential in the resulting, protonated systems is strongly dependent on the total charge of the system, the multiple protonation of the chain cannot be realistically modelled without including the presence of PA molecules in the models. Further, our main goal was to investigate the influence of the aryl-ether groups in the TZ-PEEN structure (by comparison of the 'monomer' **1b** with unsubstituted tetrazole **1a**) on the protonation, as well as the effect of neighbouring units (by comparison of the 'trimer', **1c** with the 'monomer', **1b**), and to relate the results to the comparable PBI-based models. It may be presumed that consideration of the single protonation is sufficient for this purpose. A detailed analysis of the multiple protonation for larger polymer models including PA molecules will be a subject of our future studies.

In the tetrazole-based structures, **1a-H$^+$**, **1b-H$^+$,** and **1c-H$^+$,** protonation of each of the tetrazole-nitrogen atoms was considered. It should be pointed out that for unsubstituted tetrazole protonation of the N4 and N3 positions is facile, with a negligible energetic preference of the latter (by ca. 0.1 kcal/mol). However, in **1b-H$^+$,** and **1c-H$^+$** the protonation of N4 is preferred (by ca. 8.1 kcal/mol and 7.6 kcal/mol, respectively). Therefore, in **Figure 1** only the structures

protonated at N4 position are shown. In the PBI-based structures, **2a-H⁺**, **2b-H⁺,** and **2c-H⁺**, the proton is attached to the corresponding N3 atom.

The optimized, minimum energy structures of the neutral and the protonated models are shown in parts B and D of **Figure 1**, respectively. Concerning the optimized geometries of the polymer models, it is worth emphasizing that in all the structures the tetrazole and the phenyl rings are almost co-planar in the central unit with the deviation of the torsion angle by ca. 1°-5°. The planar arrangement is stabilized by the interaction between the proton on the nitrogen atom and the ether oxygen atom(s) (intra-molecular hydrogen bonding); the (N-H)---O distance varies between 1.99-2.02 A for different structures.

Charge distribution in the neutral systems has been characterized by Hirshfeld atomic charges (**Figure 2**, part A) and the molecular electrostatic potential, MEP (**Figure 2**, part B, **Figure 3**, and **Table 2**). For all the tetrazole-based systems the most negative atomic charge (red color in **Figure 2)** is observed on N4 atom; for PBI-systems on the corresponding atom labeled as a N3, **Figure 2A**. The picture emerging from atomic charges is consistent with the MEP distribution. For tetrazole-based systems MEP exhibits a negative region extending over N2-N3-N4 part of the ring; for the PBI-systems in the vicinity of the corresponding N3 atom. Thus, it may be predicted that for tetrazole-systems the proton/positive charge will be stabilized in a relatively extended, wide negative MEP region, in proximity of N2-N3-N4. This is in agreement with earlier studies focused on tetrazole [36, 37].
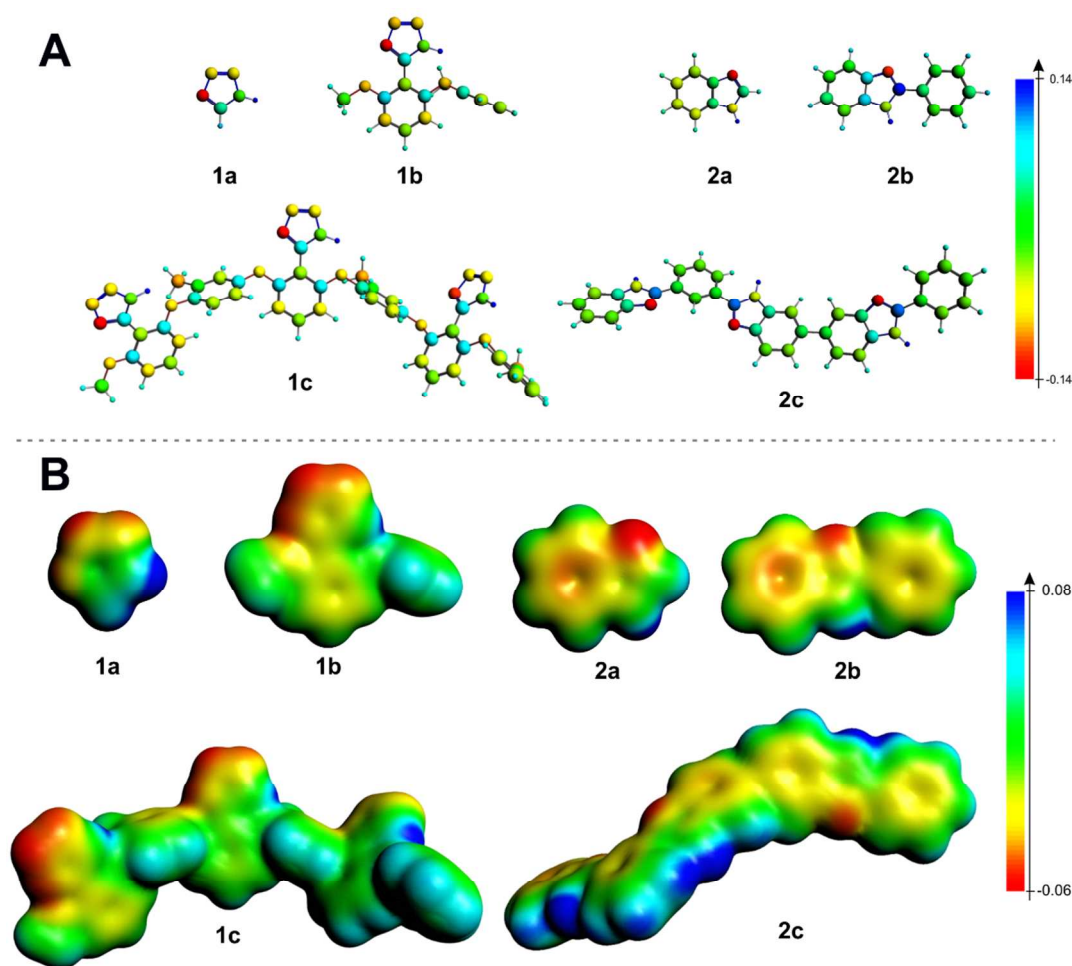
Figure 2: Panel A presents the color representation of Hirshfeld atomic charges for the considered compounds. The color scale is shown in the right side of the panel; blue color corresponds to highest positive, and red to the highest negative charge. Panel B presents Molecular Electrostatic Potential (MEP) color-coded at electron-density isosurface ($\rho = 0.002$ a.u.). In the right side of the plot the color scale is shown; blue color corresponds to highest positive MEP and red to the lowest MEP values.

It is worth pointing out, however, that the details of the MEP distribution change when comparing simple, unsubstituted tetrazole molecule and the tetrazole ring in the monomer/polymer models. Namely, the depth of the minima (**Figure 3**, **Table 2**) increases as an influence of the ether-oxygen atoms. Also, a relative depth of the minima in the vicinity of N2, N3, N4 atoms changes: for tetrazole, the N3-minimum is slightly deeper, while for **1b**, and **1c**,

the N4-minimum is the deepest. Thus, it may be expected that the preferred protonation site changes in the polymer (N4) compared to unsubstituted tetrazole (N3). In the PBI-system, the trend in MEP is opposite, when comparing unsubstituted benzimidazole **2a** and the polymer models **2b** and **2c**. Here, in the polymer models electrostatic potential becomes less negative than in the simple benzimidazole as an influence of the positive MEP in plane of the introduced phenyl ring (originating mostly from hydrogen atoms).
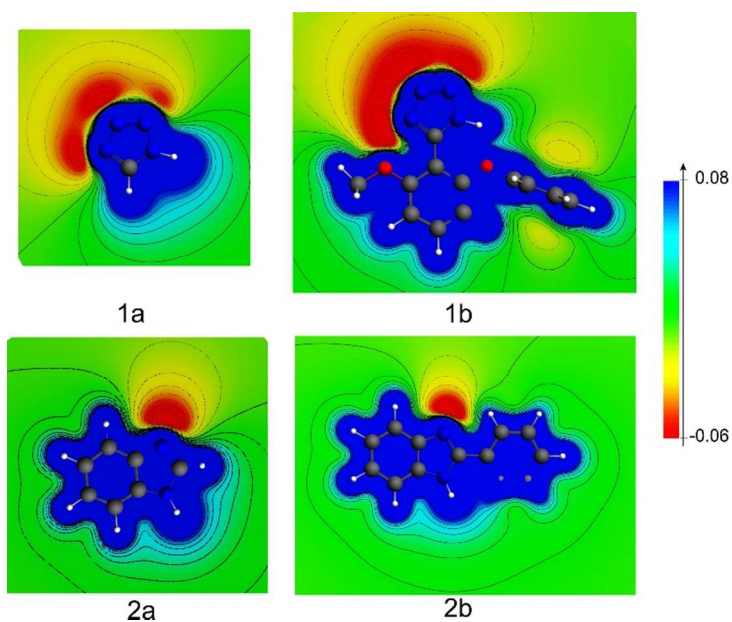
Figure 3: Contour maps of MEP for the neutral compounds plotted in the plane containing heterocyclic ring. In the right side of the plot the color scale is shown; blue color corresponds to highest positive MEP and red to the lowest MEP values.

A comparison of the experimental and previously calculated pK_a values[38] shows that imidazole will be mainly protonated in the presence of PA (pK_a (PA) = 2.15, pK_a (imidazole) = 14.52, pK_a (imidazolium) = 6.95). However, tetrazole has a pKa of 4.90, and tetrazolium ions have a pK_a of -2.68. Therefore, only a fraction of the tetrazole units will be protonated to tetrazolium ions by PA. The calculated protonation energies for all the considered models are collected in **Table 2**. The results show that comparing unsubstituted tetrazole **1a** with

benzimidazole **2a** the protonation is more stabilizing for the latter, the difference is ca. 27 kcal/mol. The protonation is facilitated in the 'monomers' compared to small molecules, and further in the 'trimers'. However, this effect is much stronger for the tetrazole-based models then for PBI. As a result, the protonation energies for tetrazole- and PBI-'monomers' are comparable (**1b** vs. **2b**); for the corresponding 'trimers' the preference of PBI is now only ca. 1 kcal/mol (**1c** vs. **2c**). These effects clearly originate from the changes in MEP discussed earlier (for tetrazole: MEP deeper for **1b**, **1c** than for **1a**, while for PBI deeper for **2a** than **2b**, **2c**). In other words, while the calculated protonation energies of tetrazole **1a** and imdazole **2a** reflect qualitatively the lower pK_a values of tetrazole, our calculations predict that the introduction of 2,6-ether substituted phenyl groups in the C5-position of tetrazole significantly increases the pK_a values of such tetrazole groups, into the range of imidazole systems. This can be understood by the predicted planar structure of these systems, which allows for resonance stabilisation over the phenyl ring. Therefore, while tetrazole based polymers may not interact well enough with PA to be doped efficiently, systems containing 2,6-ether substituted phenyl groups in the C5-position of tetrazole may be very attractive systems for PA doped polymers.

In order to further validate our main conclusion for larger models, the preliminary calculations were performed for the tetrazole model comprising four repeat units ('tetramer'), as well for the PBI models with four and six benzimidazole fragments ('dimer' and 'trimer'). The results show (see Supporting Information, Table S1) that there is no qualitative influence of the model elongation, concerning the trends in the protonation energies for the tetrazole- and PBI-based systems.

Table 2. The minimum values of the molecular electrostatic potential, V_{min}, and the protonation energies, ΔE_p,[1] in kcal/mol.

systems:	V_{min}	$\Delta E_p{}^1$
1a	-47.1 (N₄) -47.7 (N₃)²	-206.43 (-37.59)
1b	-63.4 (N₄) -60.2 (N₃)	-240.48 (-71.64)
1c	-56.5 (N₄) -55.2 (N₃)	-245.53 (-76.69)
2a	-58.4 (N₃)	-233.78 (-64.94)
2b	-53.3 (N₃)	-240.37 (-71.53)
2c	-54.6 (N₃)	-246.73 (-77.89)

[1] reaction energy for $X + H^+ \rightarrow XH^+$ and for $X + H_3O^+ \rightarrow XH^+ + H_2O$ (in brackets)

[2] two values describe the minima in the vicinity of the N3 and N4 nitrogen atoms

Finally, charge distribution in the protonated systems is presented in **Figure 4**, again based on Hirshfeld atomic charges (part A) and molecular electrostatic potential (part B). The results clearly show that the positive charge is strongly localized on the protonated units (the carbon C2 and NH atoms). Thus, it may be expected that further protonation on the non-protonated polymer units should be facile. It should be pointed out that this effect may be of vital importance for proton conductivity. However, it should be emphasized that the simple models applied in the present study are not suitable for discussion of multiple protonation. Larger, more complex models, including PA species (both, PA⁻ anions, and neutral PA molecules) are required, to investigate and compare a degree of protonation in the studied polymers, as well as to describe the effect of the protonated neighbouring units. This is beyond the scope of the present study and will be a subject of our further theoretical calculations (for some preliminary results see Supporting Information, Tables S2-S4).
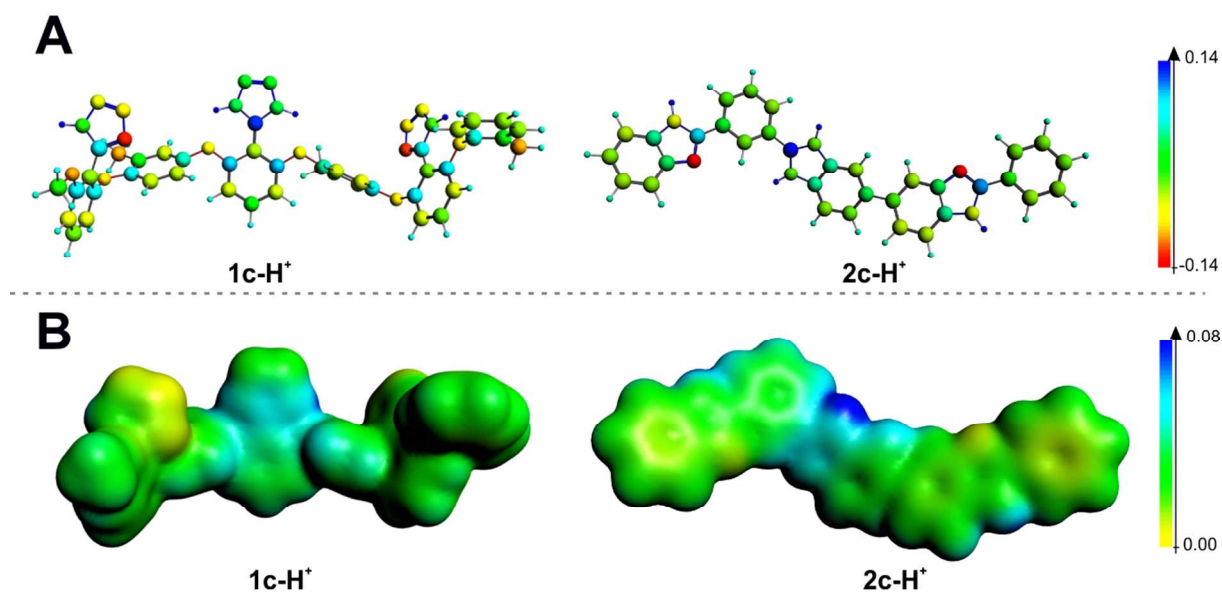
Figure 4: Panel A presents the color representation of Hirshfeld atomic charges for the protonated trimeric compounds. The color scale is shown in the right side of the panel; blue color corresponds to highest positive, and red to the highest negative charge. Panel B presents Molecular electrostatic potential (MEP) color-coded at electron-density isosurface ($\rho = 0.002$ a.u.). In the right side of the plot the color scale is shown; blue color corresponds to highest positive MEP and yellow to the lowest MEP values.

3.3 Phosphoric acid uptake of tetrazole containing membranes

To test the PA uptake of both TZ-PEEN and TZ-SPEEN, dry membrane samples were immersed in 85% PA solutions at 30, 80 and 120 °C. Every few hours, the samples were weighed and the wet weight (gross PA uptake) was noted (**Figure 5**). In general, TZ-PEEN absorbed more PA than TZ-SPEEN. While TZ-PEEN membranes reached an equilibrium value after about 10 hours, independent of the temperature, TZ-SPEEN membranes rapidly increased the weight until about 10 hours, and then continued to absorb PA at a lower rate. At 30 °C, the PA uptake decreased again after ca. 20 hours. This unexpected behaviour suggests that this membrane is not stable under acidic conditions and undergoes some chemical or morphological changes, which seem to be compensated by the strong swelling forces at elevated temperatures. The PA uptake of TZ-PEEN suddenly increased after 50 hours, up to about 270%, rendering the membrane into a sticky, gel-like membrane. Therefore, further characterisations of PA doped membranes were

done with membranes doped only for about 10-15 hours at 120 °C, giving access to doping levels of about 110 and 50 wt% for TZ-PEEN and TZ-SPEEN, respectively.
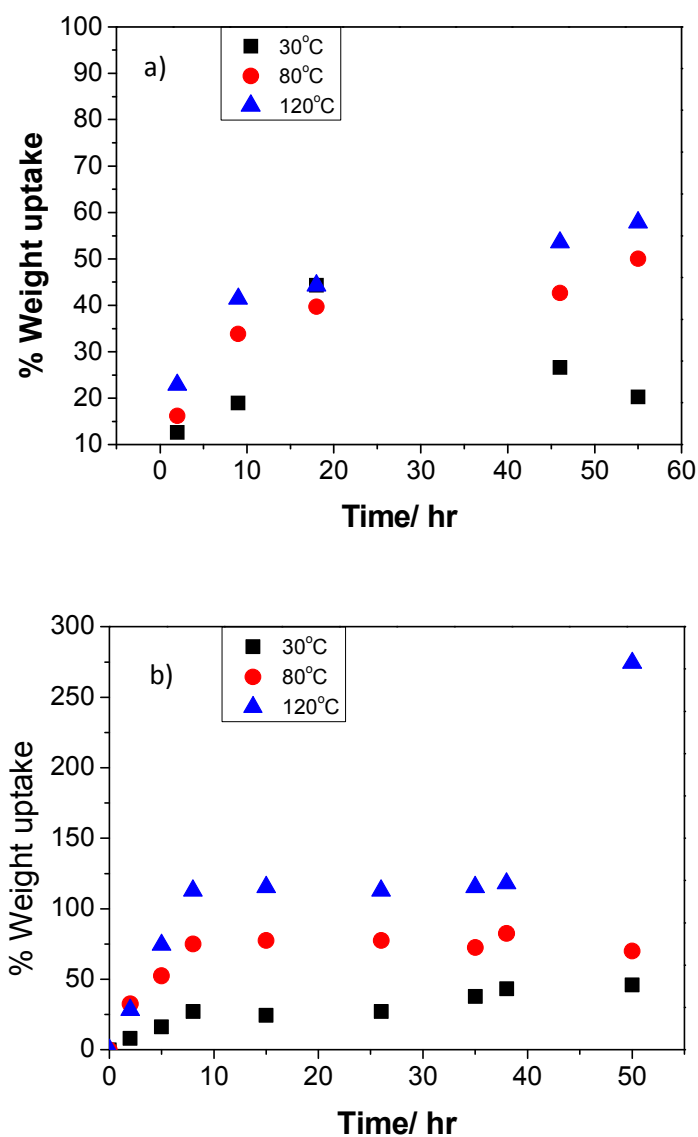
Figure 5: PA uptake of tetrazole containing membranes in 85% PA solutions at different temperatures; a) TZ-SPEEN membranes, b) TZ-PEEN membranes.

It was reported for PBI membranes that the water contents of the absorbed PA is roughly in the range of 15% of the weight gain,[39] and can be determined by drying membranes in the vacuum at 110 °C.[40] Drying of doped membranes showed that the acid inside of the membranes had a

water concentration of 24 and 14% for TZ-PEEN and TZ-SPEEN, respectively. A comparison of the equilibrium acid doping level in 85wt% PA at room temperature reveals that TZ-PEEN and *meta*-PBI[3] absorb 0.5 and 4.7 mole PA/mole heterocycle, respectively (corrected for 24 and 14% water in the absorbed PA). Clearly PBI shows a higher affinity to PA than TZ-PEEN.

3.4 Thermal stability

The thermal stability of phosphoric acid doped and pristine membranes was investigated by thermal gravimetric analysis under nitrogen atmosphere at a heating rate of 10 $^\circ$C/min. For the PA doped tetrazole membranes, TZ-PEEN and TZ-SPEEN were both doped at 120 $^\circ$C for 15-20 hours. As seen in **Figure 6**, all samples show two degradation steps. 5% weight loss was observed around 212 $^\circ$C or higher. For undoped TZ-PEEN and TZ-SPEEN, 5% weight loss was observed at 229 and 286 $^\circ$C, respectively, fulfilling the minimum temperature requirement for high temperature fuel cells.
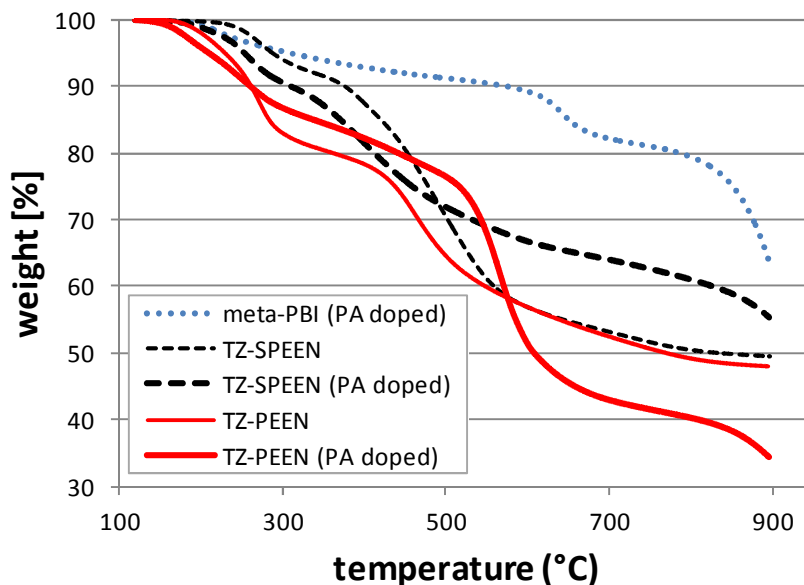
Figure 6: Thermal analysis of tetrazole containing membranes before and after PA doping at 120 °C for 15-20 hours; data for *meta*-PBI (ca 90 wt% PA uptake) from [3].

19

The origin of the first degradation step around 200 $^{\circ}$C is not clear. One possibility is residual water which could not be removed by pre-drying at 100 °C for 30 minutes, as water molecules are likely involved in intermolecular hydrogen bonding with the nitrogen atoms.[41] Another possibility is related to the tetrazole moieties. For 70% tetrazolated TZ-PEEN, loss of tetrazole would account for 19% weight loss, and loss of HN_3 (back reaction of the cycloaddition with azide) for 12%. Therefore, loss of the whole tetrazole group during thermal degradation is more probable. On the other hand, TZ-SPEEN shows only half of the expected weight loss. This may indicate a stabilising effect, e.g. ionic interaction, of the sulfonic acid groups. For acid doped samples, degradation includes dehydration of PA under formation of PA anhydrides. Around 400 $^{\circ}$C, all 4 samples show degradation of the polymer backbone.

3.5 Mechanical stability

The mechanical properties of TZ-PEEN and TZ-SPEEN and their dependence on the PA uptake were analysed by a universal testing machine. As expected, both materials showed highest tensile strength and Young's modulus in the pristine form, 72 MPa and 1.5 GPa for TZ-PEEN, and 67 MPa and 1.7 GPa for TZ-SPEEN (**Figure 7**). Absorption of phosphoric acid decreased these values, down to a tensile strength of 20 MPa and a Young's modulus of 1 GPa for TZ-PEEN with a PA uptake of 112%. Yang et al. reported a tensile strength of 25.8 MPa for *meta*-PBI with a PA uptake of 180% (Mw of PBI = 37,000 g/mol),[42] and Cho et al. reported a tensile strength of 20.4 MPa for *meta*-PBI (45,000 g/mol) with a PA uptake of 172%.[3] Considering the various factors influencing these measurements, water contents of the membranes, temperature, and molecular weight of the polymer matrix, it can be seen that the tensile strength of PA doped TZ-PEEN is just slightly lower or similar to that of commercial PBI. The Young's Moduli, however, are high for all materials, meaning that the membranes are very strong, but not tough, and therefore rather brittle. This could be an effect of low molecular weight, and even though SEC measurements of SPEEN with PMMA standards indicated a Mn of 21,100 and a Mw of 50,900 g/mol, which is reasonably high for a membrane forming polymer[42], this might still be too low, because different analytical methods were used (viscosity *vs*. SEC). TZ-SPEEN gave values of Mn = 36,800 g/mol, and a Mw of 128,000. Its Mpeak (Mp=153,700) was more than twice lower in comparison to that of *meta*-PBI (Mp=339,400). TZ-PEEN showed a Mn of 28,400 and a very high Mw value of 1,667,000

g/mol, due to the high molecular weight fraction being out of the calibration. A reason for the brittle behaviour of TZ-SPEEN could be also strong interactions of the tetrazole groups by hydrogen bonding, which may only be partially interrupted by protonation in the PA doped systems, because tetrazolium ions still possess unprotonated nitrogen atoms which act as hydrogen bond acceptors. Furthermore, as discussed before, while imidazole is mainly protonated in the presence of PA, the tetrazole units in TZ-PEEN and TZ-SPEEN are probably not fully protonated, due to the low pK_a values of tetrazole and tetrazolium. A lower level of protonation than observed for PBI is also indicated by the behaviour of DMAc/0.5 wt.-% LiCl solutions, used as eluent for SEC. While the SEC curve of TZ-SPEEN does not show any dependence on the concentration of the polymer (from 0.5-12 mg/ml, data not shown), this is not true in case of *meta*-PBI - its chain collapses after a concentration of 2-4 mg/ml, forming compact structures with changed conformation, which results in the shift of SEC curves to higher elution volumes, i.e. lower molar masses. [43].
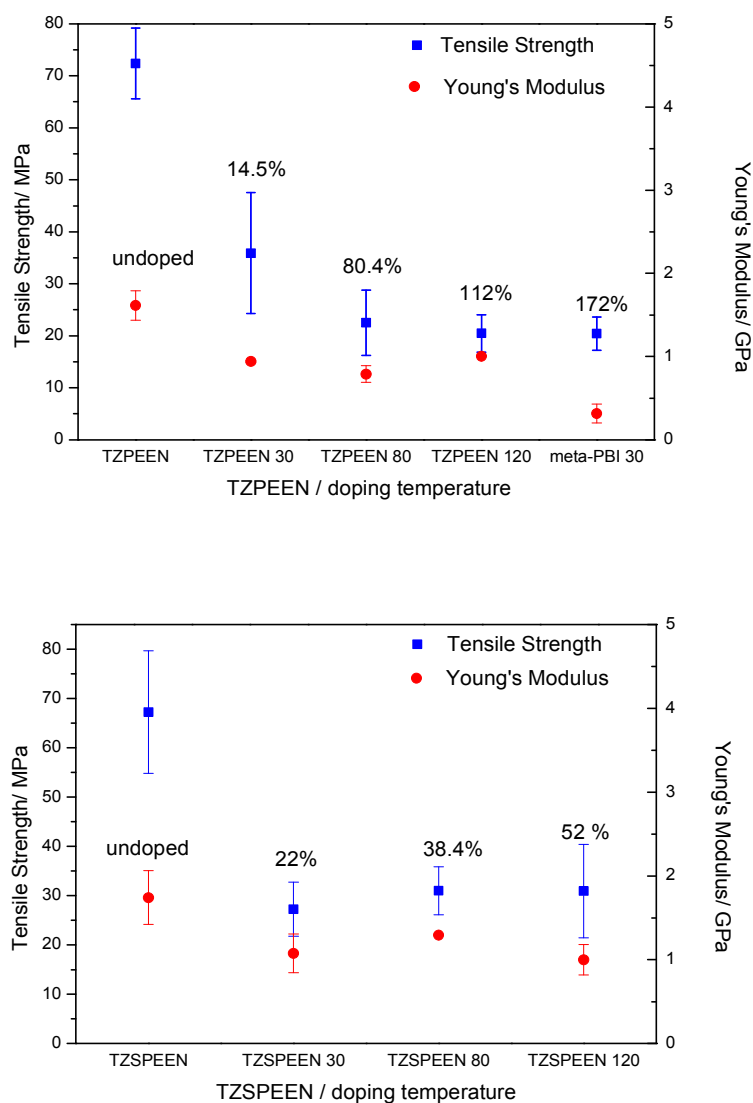
Figure 7: Tensile Strength and Young's Modulus of membranes doped in 85% PA with different PA uptake (noted in the figure); temperature: 27 °C, relative humidity: 31%. Data for *meta*-PBI (doped in 70% PA) are from [3].

3.6 Ionic conductivity

For measuring in-plane proton conductivity, one TZ-SPEEN membrane sample and three TZ-PEEN samples cut from the same membrane were prepared by doping in 85 wt% PA at 120 °C for 15-20 hours. After doping the membranes were dried at 110 °C for 5 hours in the vacuum.

The membrane weight gains due to the doping acid were found to be of 81%, 109% and 112% (TZ-PEEN) and 58% (TZ-SPEEN). Drying of the obtained membranes before measuring the conductivity ensured that the measured conductivity is that of dry membranes, because water increases the conductivity of PA doped membranes.[2] The proton conductivities of PA doped tetrazole-based membranes (**Figure 8**) were then studied using electrochemical impedance spectroscopy (EIS). Compared with the proton conductivity of PA-doped *meta*-PBI with a weight gain of 172% during doping, TZ-PEEN membranes show much better values: At 160 ^{o}C, the proton conductivity of PA-doped *meta*-PBI was reported as 14 mS/cm [3] while TZ-PEEN shows a conductivity of about 25 mS/cm, even though the PA uptake is lower. Considering the lower doping level of TZ-SPEEN in comparison to TZ-PEEN, it can be expected that the conductivity of TZ-SPEEN is much lower, and indeed it only reaches 12 mS/cm at 160 °C, similar to that of the mentioned *meta*-PBI membrane, but at 30% of the acid uptake. Of course these values are very low in comparison with state-of-the-art membranes, e.g. *meta*-PBI doped with a PA uptake of about 350 wt% showed a conductivity of 130-140 mS/cm at the same temperature,[42] but since reduction of the PA uptake increases the mechanical stability, some researchers try to reduce the PA uptake.[34] In the Arrhenius plot, the PA doped membranes show an inflection point at around 120 °C (**Figure S5**). Between 60-100 °C, however, a reasonably linear trend is observed (R^2 > 0.99), indicating that proton conduction in PA doped TZ-PEEN and TZ-SPEEN has an activation energy in the range of 35 kJ/mol. According to the literature, the activation energy for proton conduction in various PBI derivatives increases with increasing acid content, independent of the exact chemical structure of the polymer matrix, reaching about 45 kJ/mol at an acid content of 60% (**Figure S6**).[44] Even though the acid content in TZ-PEEN and TZ-SPEEN is lower (37 - 53 %), the activation energies observed for tetrazole based membranes are much lower. This suggests that proton conduction in the presented materials follows another mechanism, e.g. this could be a strong contribution of proton hopping involving the tetrazole rings, as already suggested for some non-doped tetrazole containing polymers.[12] In summary, it seems that tetrazole based membranes have an intrinsically higher conductivity, which should increase further if it is possible to increase the acid uptake without degrading the mechanical stability, e.g. by a mechanical reinforcement.
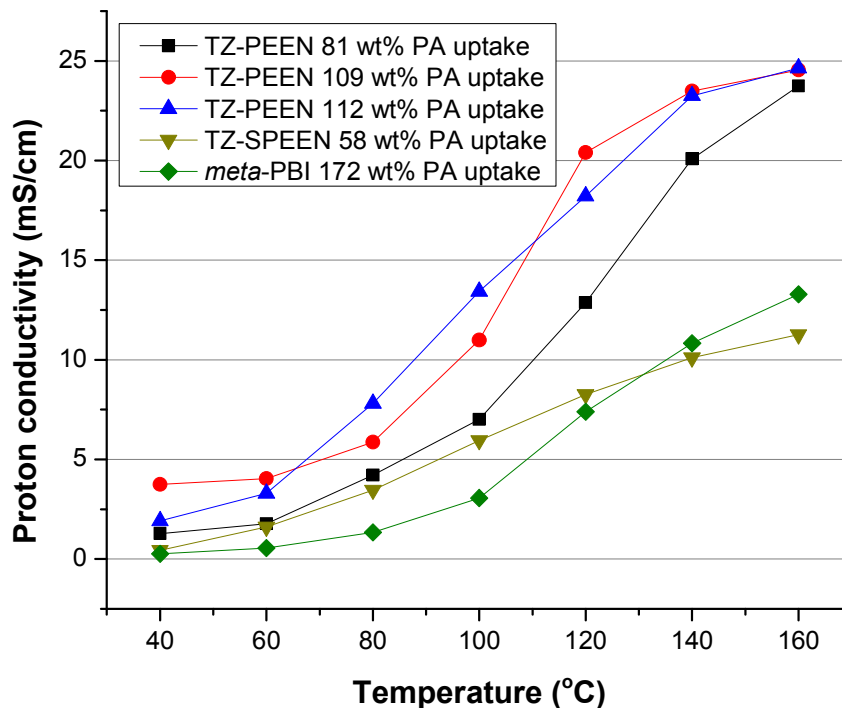
Figure 8: In-plane conductivity of PA doped TZ-PEEN and TZ-SPEEN membranes; doping conditions: 120 °C, 85 wt% PA solution, 15-20 hours. Data for *meta*-PBI are from [3].

3.7 Fuel cell tests

To evaluate tetrazole based membranes in the fuel cell, one TZ-SPEEN membrane (40 μm thick, **MEA1**) and two TZ-PEEN membranes (52 and 72 μm thick, **MEA2** and **MEA3**) were doped for ca. 20 hours at 50 °C (TZ-PEEN) and 120 °C (TZ-SPEEN), resulting in a weight gain of 46-51% (TZ-PEEN) and 56% (TZ-SPEEN). The membranes swelled mainly in the thickness during doping, and were directly assembled into a fuel cell without additional drying steps.

3.7.1 TZ-SPEEN fails rapidly in the fuel cell

Following our standard procedure, **MEA1** was operated at a current density of 200 mA/cm^2 for activation. During activation, redistribution of PA typically increases the cell potential until a steady value is reached. For TZ-SPEEN membranes, however, the potential decreased rapidly and already after 4 hours reached 0V (red, upper curve in **Figure S7**). The reason for the observed catastrophic failure is the low acidic stability of bisphenol A that can lead to scission of the polymer main chain.[45, 46] SEC analysis of the failed membrane confirmed this hypothesis (supporting information) .

3.7.2 TZ-PEEN shows good performance in the fuel cell

Both TZ-PEEN membranes showed a stable fuel cell performance at 160 °C and a current density of 200 mA/cm^2, indicating that indeed the bisphenol A unit in TZ-SPEEN acts as a breaking point. After activation, **MEA2**, based on 52 μm thick TZ-PEEN, showed a peak power density of 287 mW/cm^2 and a potential at 200 mA/cm^2 of 558 mV (**Figure 9**). Linear sweep voltammetry (**Figure S10**) revealed that **MEA 2** was practically free of electric shorting (slope of the linear part ~ 0 Ω^{-1} cm^{-2}), and that the hydrogen crossover current was in the range of 10 mA/cm^2 (extrapolation to 0 V). This crossover current density is too large for practical applications, but can be improved by increasing the membrane thickness and probably also by optimisation of the membrane casting process.
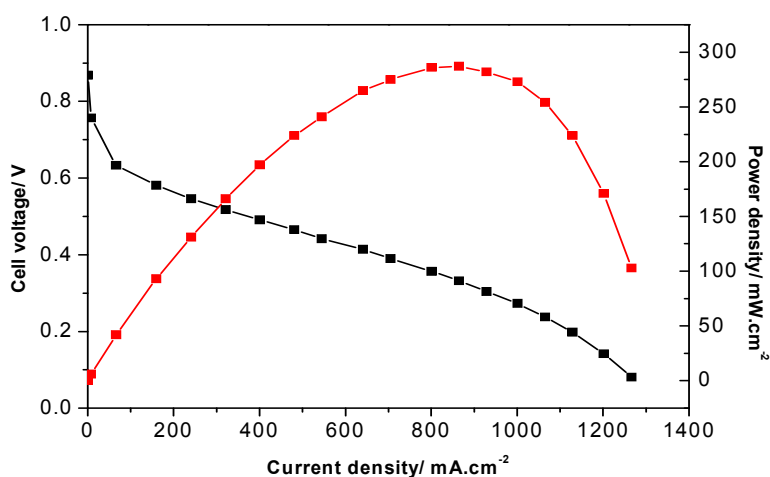
Figure 9: Polarization curve and power density curve of **MEA2**, a 52 μm thick TZ-PEEN membrane, doped to a PA uptake of 46% PA (wet); cell temperature 160 °C.

As expected, the thicker **MEA3** had a lower peak power density and potential at 200 mA/cm^2 than **MEA2** (**Figure 10**). The break-in time was very short, and the cell practically immediately reached a state of constant performance (**Figure 11**). After 96 hours at constant current, the cell was disassembled to test another MEA. Then **MEA3** was re-assembled, and again run at constant current until 208 hours operation were reached. The initially improved performance after reassembly can be explained by the absorption of free water from the atmosphere, which reduces the viscosity of the PA in the membrane and thus lowers the MEA's resistance. When the current density was increased to 600 mA/cm^2, the cell operated stable for over 100 hours, until a sudden drop in potential ended the test after 325 hours operation. Reasons for the failure are unclear. Since high current densities lead to concentration of PA at the anode by movement of phosphate anions, and eventually loss of PA,[47] it seems possible that loss of PA led to shrinking induced stresses in the membrane, and finally to mechanical failure. Further analysis into this matter was not possible, because the membrane strongly adhered to both GDEs after disassembly.
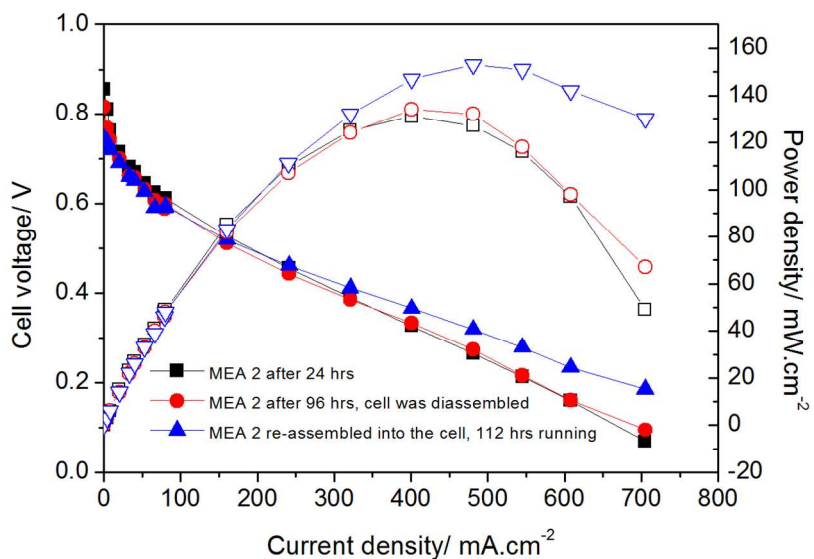
Figure 10: Polarization curve and power density curves of **MEA3,** a 72 μm thick TZ-PEEN membrane, doped to a PA uptake of 51% PA (wet); cell temperature 160 °C.
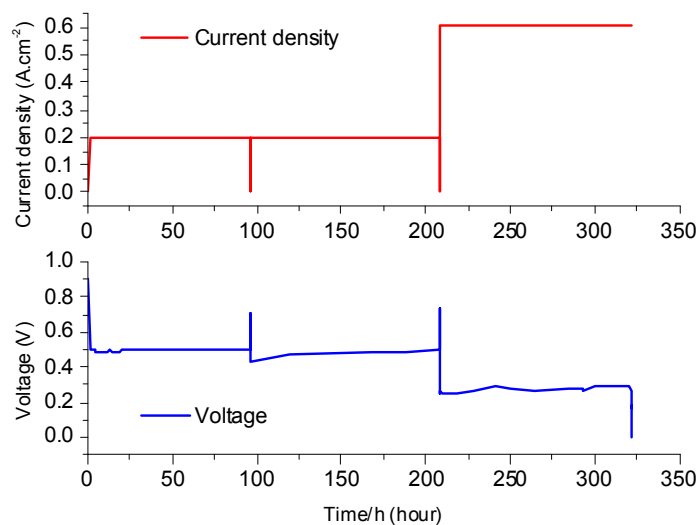
Figure 11: Development of the potential during the fuel cell test of **MEA3**. At 96 hours, the cell was disassembled and reassembled. After 208 hours, the current density was increased to 0.6 A/cm^2, leading to a sudden failure around 325 hours.

4. Conclusions

DFT calculations predict that tetrazole systems with 2,6-ether substituted phenyl groups in the C5-position are coplanar systems, allowing for resonance stabilisation. This is expected to increase the pK_a values into the range of imidazole systems, allowing for efficient PA doping, while still providing two potential sites for proton hopping, as suggested by molecular electrostatic potential (MEP) calculations. Polymers with tetrazole pendant groups were obtained by reacting nitrile containing polymers with sodium azide. While bisphenol A based polymer backbones were chemically unstable under phosphoric acid doped conditions, aromatic poly(ether) based TZ-PEEN was stable and could be doped up to a PA uptake of about 110%. At room temperature, TZ-PEEN and *meta*-PBI[3] showed an equilibrium uptake of 0.5 and 4.7 mole PA/mole heterocycle, indicating that PBI has a higher affinity to PA then TZ-PEEN. Nevertheless, TZ-PEEN doped to 110% PA uptake showed a proton conductivity close to 25 mS/cm at 160 °C with a remarkably low activation energy of about 35 kJ/mol. Furthermore, a peak power density of 287 mW/cm^2 was obtained at 160 °C in a fuel cell test which was not optimised for this class of polymers (catalyst load, cell compression, test procedure etc.). To our knowledge, this is the highest operating temperature reported so far for tetrazole based systems. Taking all these findings into account, it seems possible that tetrazole based systems can be a way towards materials showing high proton conductivity at low PA contents. This work opens a large space for future work, including polymer optimisation: e.g. linker length (in this paper TZ was directly bonded to the polymer), bonding site (here C5), optimisation of the MEAs, etc.

5. Acknowledgements

6. References

[1] F. Zhou, S. S. Araya, I. F. Grigoras, S. J. Andreasen, S. K. Kær, *J. Fuel Cell Sci. Tech.*, **2015**, *12*, 021002 (1-9).

[2] J. S. Wainright, J.-T. Wang, D. Weng, R. F. Savinell, M. Litt, *J. Electrochem. Soc.* **1995**, *142,* L121-L123.

[3] H. Cho, E. Hur, D. Henkensmeier, G. Jeong, E. Cho, H.-J. Kim, J. H. Jang, K.-Y. Lee, H. A. Hjuler, Q. Li, J. O. Jensen, L. N. Cleemann, *Eur. Polym. J.* **2014**, *58*, 135–143.

[4] L. Xiao, H. Zhang, E. Scanlon, L. S. Ramanathan, E.-W. Choe, D. Rogers, T. Apple, B. C. Benicewicz, *Chem. Mater.* **2005**, *17*, 5328-5333.

[5] Q. Li, J. O. Jensen, R. F. Savinell, N. J. Bjerrum, *Progr. Polym. Sci.* **2009**, *34*, 449–477.

[6] N. Gourdoupi, J. K. Kallitsis and S. Neophytides, *J. Power Sources* **2010**, *195*, 170-174.

[7] C. Morfopoulou, A. K. Andreopoulou and J. K. Kallitsis, *J. Polym. Sci., Part A: Polym. Chem.* **2011**, *49*, 4325-4334.

[8] C. I. Morfopoulou, A. K. Andreopoulou, M. K. Daletou, S. G. Neophytides, J. K. Kallitsis, *J. Mater. Chem. A* **2013**, *1*, 1613-1622.

[9] J. Yang, Q. Li, J. O. Jensen, C. Pan, L. N. Cleemann, N. J. Bjerrum, R. He, *J. Power Sources* **2012**, *205*, 114– 121.

[10] M. M. Nasef, dx.doi.org/10.1021/cr4005499

[11] H.-T. Pu, S. Ye, React. Funct. Polym. **2006**, *66*, 856–862.

[12] H. Pu, J.Wu, D. Wan, Z. Chang, *J. Membr. Sci.* **2008**, *322*, 392–399.

[13] M.-K. Song, H. Li, J. Li, D. Zhao, J. Wang, M. Liu, *Adv. Mater.* **2014**, *26*, 1277-1282.

[14] E. Kim, P. F. Weck, N. Balakrishnan, C. Bae*, J. Phys. Chem. B* **2008**, *112*, 3283-3286.

[15] N. Idupulapati, R. Devanathan, M. Dupuis, *J. Phys. Chem. A* **2010**, *114*, 6904–6912.

[16] Y. Zhou, J. Yang, H. Su, J. Zeng, S. P. Jiang, W. A. Goddard, *J. Am. Chem. Soc.* **2014**, *136*, 4954−4964.

[17] N. Du, G. P. Robertson, M. M. Dal-Cin, L. Scoles, M. Guiver, *Polymer* **2012**, *53*, 4367 – 4372.

[18] A. D. Becke, *Phys. Rev. A* **1988,** *38*, 3098-3100.

[19] J. P. Perdew, *Physical Review B: Condensed Matter and Materials Physics* **1986,** *34*, 7406-7406.

[20] J. P. Perdew, *Phys. Rev. B* **1986,** *33*, 8822-8824.

[21] G. te Velde, F. M. Bickelhaupt, E. J. Baerends, C. Fonseca Guerra, S. J. A. van Gisbergen, J. G. Snijders, T. Ziegler, *J. Comput. Chem.* **2001,** *22*, 931-967.

[22] E. J. Baerends, D. E. Ellis, P. Ros, *Chem. Phys.* **1973,** *2*, 41-51.

[23] E. J. Baerends, P. Ros, *Chem. Phys.* **1973,** *2*, 52-59.

[24] G. te Velde, E. J. Baerends, *J. Comput. Phys.* **1992,** *99*, 84-98.

[25] C. G. Fonseca Guerra, O. Visser, J. G. Snijders, G. te Velde, E. J. Baerends, *Methods and Techniques in Computational Chemistry: METECC-95*. STEF: Cagliari, Italy, **1995,** p. 303.

[26] E. van Lenthe, E. J. Baerends, J. G. Snijders, *J. Chem. Phys.* **1993,** *99*, 4597-4610.

[27] E. van Lenthe, E. J. Baerends, J. G. Snijders, *J. Chem. Phys.* **1994,** *101*, 9783-9792.

[28] F. L. Hirshfeld, *Theoret. Chim. Acta* **1977**, *44*, 129–138.

[29] J. S. Murray, P. Politzer, *WIREs Comput Mol Sci* **2011**, *1*, 153-163.

[30] J. S. Murray, P. Politzer, *Theoretical Chemistry Accounts* **2002**, *108*, 134-142.

[31] D. Cantillo, B. Gutmann, C. O. Kappe, *J. Org. Chem.* **2012**, *77*, 10882−10890.

[32] D. Cantillo, B. Gutmann, C. O. Kappe, *J. Am. Chem. Soc.* **2011**, *133*, 4465–4475.

[33] M. Girardin, S. J. Dolman, S. Lauzon, S. G. Ouellet, G. Hughes, P. Fernandez, G. Zhou, P. D. O'Shea, *Org. Process Res. Dev.* **2011**, *15*, 1073–1080.

[34] D. C. Villa, S. Angioni, S. Dal Barco, P. Mustarelli, E. Quartarone, *Adv. Energy Mater.* **2014**, *4*, 1301949 (1-8).

[35] A. Dişli, M. Salman, Russ. *J. Org. Chem.* **2009**, *45*, 151-153.

[36] F. H. Allen, C. R. Groom, J. W. Liebeschuetz, D. A. Bardwell, T. S. G. Olsson, P. A. Wood, *J. Chem. Inf. Model.* **2012**, *52*, 857−866.

[37] D. D. Zorn, J. A. Boatz, M. S. Gordon, *J. Phys. Chem. B* **2006**, *110*, 11110-11119.

[38] J. F. Satchell, B. J. Smith, *Phys. Chem. Chem. Phys.* **2002**, *4*, 4314–4318.

[39] X. Glipa, B. Bonnet, B. Mula, D. J. Jones, J. Rozière, *J. Mater. Chem.* **1999**, *9*, 3045-3049.

[40] Q. Li, R. He, R. W. Berg, H. A. Hjuler, N. J. Bjerrum, *Solid State Ionics* **2004**, *168*, 177-185.

[41] N.W. Brooks, R.A. Duckett, J. Rose, I.M. Ward, *Polymer* **1993**, *34*, 4039.

[42] J. S. Yang, L. N. Cleemann, T. Steenberg, C. Terkelsen, Q. Li, J. O. Jensen, H. A. Hjuler, N. J. Bjerrum, R. He, *Fuel Cells* **2014**, *14*, 7-15.

[43] C. B. Shogbon, J.-L. Brousseau, H. Zhang, B. C. Benicewicz, Y. A. Akpalu, *Macromolecules*, **2006**, *39*, 9409-9418.

[44] J. A. Asensio, E. M. Sánchez, P. Gómez-Romero, *Chem. Soc. Rev.* **2010**, *39*, 3210–3239.

[45] W. Chen, H. Lin, *Org. Lett.* **2004**, *14*, 2341-2342.

[46] S. Hink, N. M. H. Duong, D. Henkensmeier, J. Y. Kim, J. H. Jang, H.-J. Kim, J. Han, S.-W. Nam, *Solid State Ionics,* **2015**, *275*, 80-85.

[47] S. H. Eberhardt, M. Toulec, F. Marone, M. Stampanoni, F. N. Büchi, T. J. Schmidt, *J. Electrochem. Soc*. **2015**, *162*, F310-F316.